ELSEVIER

Journal of Alloys and Compounds 275–277 (1998) 877–885

Journal of ALLOYS AND COMPOUNDS

Oxygen storage and catalytic NO removal promoted by CeO_2-containing mixed oxides

R. Di Monte, P. Fornasiero, M. Graziani, J. Kašpar*

Dipartimento di Scienze Chimiche, Università di Trieste, Via L. Giorgieri 1, Trieste I-34127, Italy

Abstract

CeO_2–ZrO_2 mixed oxides show improved redox properties as compared to CeO_2 which makes them important innovative materials for three-way catalysts. The origin of this effect and the structural/redox correlation are discussed. The influence of the improved redox capacities on the reduction of NO by CO catalyzed by Rh/CeO_2–ZrO_2 catalysts is reported and evidence for an active role of the CeO_2–ZrO_2 support in NO activation is presented. © 1998 Elsevier Science S.A.

Keywords: CeO_2–ZrO_2 mixed oxides; NO removal; Oxygen storage

1. Introduction

The catalytic treatment of motor vehicle automotive exhaust gas is one of the major problems concerning pollution control. It is estimated that about 20% of polluting emissions originates from this source. Since 1975, in the USA, automotive catalytic converters have been adopted to control the emissions of internal combustion engines: at present, the so-called three-way catalyst is employed (TWC, the name derives from its ability to remove simultaneously the three categories of pollutants, i.e. CO, hydrocarbons and NO). Such a system has proved to be very effective in removing the pollutants from exhaust, however the performance of a three-way catalyst critically depends on the air/fuel ratio employed in the engine. The highest conversion of pollutants is attained close to the stoichiometric conditions, while excursions to fuel-rich (net reducing) or fuel-poor (net oxidizing) air/fuel ratios severely decreases the efficiency of TWCs. Such excursions may present a serious limitation for TWC since the air-to-fuel ratio (A/F) oscillates significantly around the stoichiometric ratio A/F=14.6. The addition of CeO_2 may limit this disadvantage due to its ability to act as an oxygen buffer by storing/releasing O_2. The higher the oxygen storage/release capacity (OSC) of the catalyst, the higher the conversion efficiency and resistance to thermal aging is generally observed. Another major problem of the present converters is the fact that significant conversion is attained only at high temperatures (>600–630 K). As a result, during cold-start of the engine, the emissions of pollutants are quite high until the converter reaches the operating temperature. Notwithstanding the good performance of commercial converters, the increasingly stringent restrictions on emissions and the inclusion of the cold-start into the converter performance test cycle will require the development of new systems. High activity, high OSC at low temperatures and high thermal stability are the targets for research [1]. In the present paper, the redox behavior of CeO_2–ZrO_2-based systems and their application to the NO–CO reaction is addressed. The latter reaction was chosen as a model reaction to test the TWC activity.

2. Experimental

CeO_2–ZrO_2 was synthesized according to previously published procedures using either Ce/Zr alkoxides or by complexing Ce/Zr nitrates with citric acid to produce an homogeneous gel which was then dried and calcined at 773 K for 5 h [2–4]. The supports were impregnated with $RhCl_3 \cdot nH_2O$, Na_2PtCl_6 and $PdCl_2$ by the incipient wetness method. The nominal metal loading was 0.5 wt%. Temperature programmed reduction and oxygen uptake measurements were carried out as previously described [2]. The catalytic reduction of NO by CO was carried out in a flow reactor as described previously [5]. The absence of diffusional limitations was accurately checked. The separation of reactants and products (NO, CO, N_2O, N_2 and CO_2) was achieved on an on-line GLC using Hayesep A

*Corresponding author.

PII: S0925-8388(98)00476-9

and Porapak Q columns. The presence of O_2 in the reactor outlet could be detected to the ppm level.

3. Results and discussion

3.1. CeO_2–ZrO_2 solid solutions as advanced OSC systems

As recalled above the OSC of CeO_2 is of fundamental importance for the effectiveness of a TWC. In pure CeO_2, the Ce^{4+}/Ce^{3+} redox process is essentially limited to the surface up to 620–670 K [6,7]. It is desirable for TWCs to be effective at temperatures as low as possible and, therefore, a high surface area is an essential prerequisite for obtaining good efficiency of the Ce^{4+}/Ce^{3+} redox cycle, i.e. high OSC. The redox behavior of CeO_2 strongly depends on the textural properties because a decrease of surface area depresses all the surface related redox processes [7]. Of the two processes concerned with the OSC, the oxidation is facile and occurs at room temperature (RT) [6–8], while the reduction of ceria starts at about 473 K and is essentially limited to the uppermost layer of the oxide up to 620–670 K [7]. Most studies concerning the OSC of CeO_2 are therefore focused on the reduction process. The temperature programmed reduction (TPR) of high surface area CeO_2 is characterized by two reduction peaks at 790 and 1100 K. The reduction of CeO_2 has been investigated thoroughly and most previous investigations agree on the attribution of these peaks to surface and bulk reduction, respectively [9], even if the formation of non-stoichiometric CeO_{2-x} phases [7] and/or the formation of hydrogen bronzes [10] cannot be excluded. Above 623 K, the CeO_2 surface is unstable in the presence of H_2 and a collapse of the surface area, due to pore filling, occurs concurrently with reduction [8]. Accordingly, when CeO_2 (surface area 194 $m^2\,g^{-1}$) after TPR was oxidized at 700 K and then subjected to further TPR, no reduction was observed below 900 K, indicating that the loss of surface area, which typically decreases below 10 $m^2\,g^{-1}$ after a TPR run, brings about a suppression of OSC at moderate temperatures [2]. This result stresses the fact that high thermal stability is an essential requirement for good OSC in CeO_2-containing supports. A close coupled location of the converter is nowadays employed in automotive applications and the TWCs experience temperatures up to 1200 K. This situation has led to considerable effort in the research for alternative OSC materials of very high thermal stability suitable for modern TWCs.

Evidence for the importance of ZrO_2 in modifying the redox behavior of CeO_2 was first reported in the open literature by Japanese authors [11,12]. The formation of CeO_2–ZrO_2 mixed oxides by a coprecipitation method decreased the temperature of the reduction in the bulk from 1100 K to about 900 K [12]. This was attributed to the high oxygen mobility in the bulk of the oxide induced by the insertion of ZrO_2 into the CeO_2 lattice. Subsequently, we reported an even more surprising observation [13]: reduction occurred at very mild temperatures (600–700 K) in the bulk of Rh-loaded CeO_2–ZrO_2 solid solutions prepared by a solid state synthesis, e.g. by firing a mixture of oxides at 1873 K, despite their extremely low surface area (LSA, $\approx$1 $m^2\,g^{-1}$). This is exemplified in Fig. 1 (traces 1–4), which shows the TPR profiles for Rh-loaded and metal-free CeO_2 and $Ce_{0.6}Zr_{0.4}O_2$.

The contribution of the surface to the reduction profile is negligible in these samples and therefore the peaks observed above 500 K are all associated with reduction of Ce^{4+} in the bulk. This was also confirmed by XANES spectra recorded at the Ce L_{III} edge, which showed strong features attributable to Ce^{3+} after reduction of Rh/$Ce_{0.6}Zr_{0.4}O_2$. The peaks below 500 K are attributed to the reduction of the Rh_2O_3 precursor. Noteworthy is the modification of the TPR profile in Rh-loaded $Ce_{0.6}Zr_{0.4}O_2$ compared to Rh/CeO_2, i.e. the appearance of a strong reduction feature centered at 670 K. This feature is attributed to promotion of reduction in the bulk of the solid solution. The insertion of ZrO_2 into the CeO_2 lattice clearly facilitates the reduction process in noble metal-loaded $Ce_{0.6}Zr_{0.4}O_2$ compared to all other samples (Fig. 1, traces 1–3). This promotion is attributed to the presence of the supported metal which activates the reducing agent (H_2) spilling it over the support favoring its reduction.

As mentioned above, a high surface area is considered to be an essential requirement for an efficient TWC. In the absence of diffusional effects, the surface reaction is normally rate limiting, hence a high surface area is desirable. In contrast, the observation that an extremely sintered material can act as an efficient oxygen storage/release system with a chemical/redox activity comparable to or even better than that of high surface area (HSA) CeO_2, suggests that tuning of the bulk properties by an appropriate structural design can make the bulk of the material available for this kind of chemical reaction.

Accordingly, we prepared a series of $Ce_xZr_{1-x}O_2$ LSA

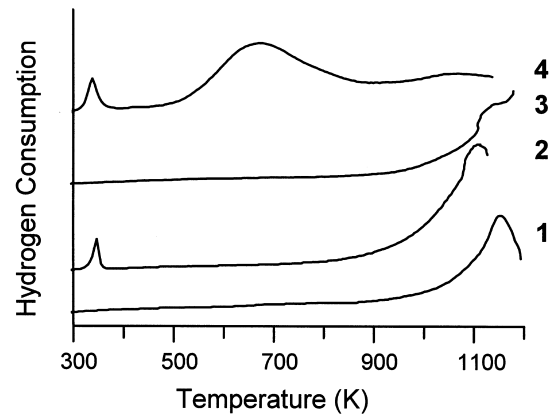

Fig. 1. Temperature programmed reduction profiles of (1) CeO_2, (2) 0.5 wt% Rh/CeO_2, (3) $Ce_{0.6}Zr_{0.4}O_2$, and (4) 0.5 wt% Rh/$Ce_{0.6}Zr_{0.4}O_2$.

samples by varying x ($0 \leq x \leq 1$) and compared their redox behavior [14]. The dependence of the temperature of reduction of the support in the bulk on the ZrO_2 content is reported in Fig. 2. Two trends are discerned from Fig. 2: (i) an increase in ZrO_2 content reduces the reduction temperature in the cubic region ($ZrO_2 \leq 50\%$) of the CeO_2–ZrO_2 phase diagram[1]; (ii) the reverse is true in the tetragonal region ($ZrO_2 \geq 50\%$). The favorable effect of the cubic phase over the tetragonal phase is evidenced by the difference in reduction temperatures observed for the two (cubic and tetragonal) $Rh/Ce_{0.5}Zr_{0.5}O_2$ LSA samples. Since H_2 activation is easy in the presence of the supported noble metal, it appears reasonable that oxygen transport from the bulk to the outer surface is rate limiting for the reduction process. A detailed structural characterization of these solid solutions by XRD, Raman and EXAFS techniques [14,15] suggests fundamental redox properties–structural relationships for CeO_2–ZrO_2 solid solutions. The insertion of progressively increasing amounts of ZrO_2 into the CeO_2 fluorite lattice up to 50 mol% is responsible for (i) a decrease of the lattice parameter, due to the smaller Zr^{4+} (0.80 Å) compared to Ce^{4+} (0.97 Å) [14]; (ii) an increase in the channel diameter for oxygen migration in the lattice; (iii) a progressive increase of structural defects; (iv) a decrease in the number of nearest neighbor oxygens around Zr^{4+} from eight to six for $Ce_{0.5}Zr_{0.5}O_2$; (v) no variation of the Ce–O coordination sphere except for some shortening of the Ce–O bond length consistent with contraction of the cell parameter. Given the stoichiometry of CeO_2–ZrO_2 solid solutions, the apparent decrease of the coordination number was attributed to high structural disorder of the ''missed'' oxygens induced by the insertion of ZrO_2 [15]. These two ''invisible'' oxygens are located at a Zr–O bond distance >2.7 Å, suggesting a large oxygen lability.

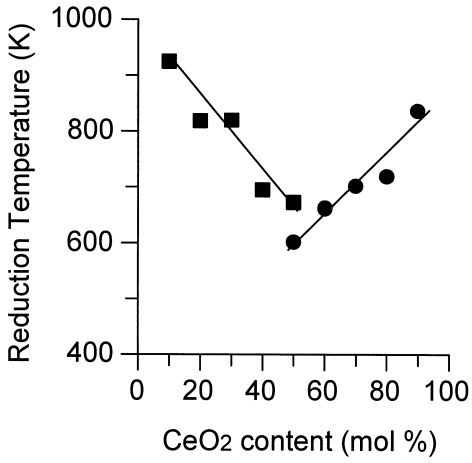

Fig. 2. Peak temperatures for the reduction of the support in the $Rh/Ce_xZr_{1-x}O_2$ ($x = 0.1$–1) LSA (2) (●) c and t″, (■) t and t′ phases.

[1]For a discussion of the CeO_2–ZrO_2 phase diagram compare Refs. [2,35,36].

A different situation is found in the tetragonal region, e.g. for $ZrO_2 \geq 50$ mol%. Here, ZrO_2 becomes the dominant factor for the nature of the phase. The Zr–O bonds now assume the typical geometry of tetragonal zirconias, e.g. four short and four long Zr–O bonds, indicating that the structural disorder found in the cubic phase is no longer present. Consistently, the amount of lattice defects remains constant in the tetragonal region [14]. The progressive tetragonalization with increasing amount of ZrO_2 now provides an effective route for the release of the lattice stress induced by ZrO_2 insertion, resulting in a lower oxygen mobility. All these results clearly indicate that oxygen mobility in the lattice is a key factor in determining Ce^{4+} reduction in the bulk of sintered CeO_2–ZrO_2 solid solutions.

The dependence of the reduction behavior of CeO_2–ZrO_2 mixed oxides upon textural properties is rather intriguing. For example, for $Ce_{0.5}Zr_{0.5}O_2$ mixed oxide the following TPR behavior was observed: a single peak at 950 K [12] and two peaks at 880 and 1000 K for a surface area of, respectively, 22 and 64 $m^2\,g^{-1}$ [2]. In another investigation two peaks at 800 and 1000 K were observed [16]. In contrast, the ultimate degree of reduction is approximately constant, e.g. $Ce_{0.5}Zr_{0.5}O_{1.85}$ is obtained after reduction at 1273 K [2,16]. Further, treatment under H_2 in the TPR leads to strong sintering of the mixed oxides and the surface area decreases to $\leq 10\ m^2\,g^{-1}$, which, as shown in Fig. 3, leads to a decrease of the reduction temperature compared to the fresh, high surface

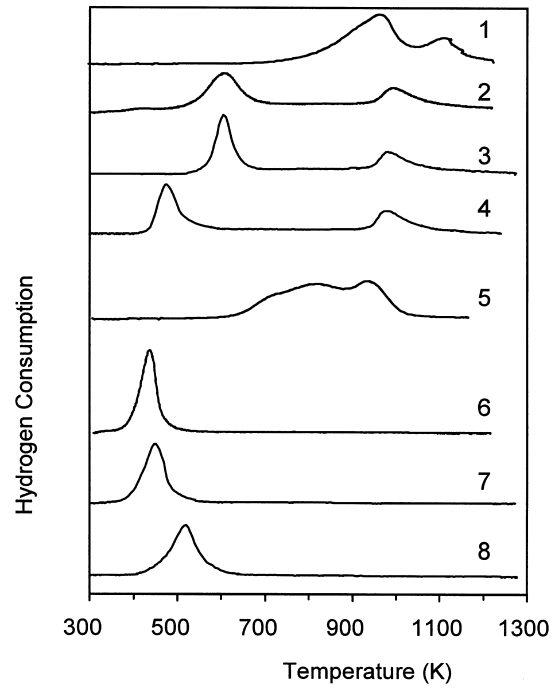

Fig. 3. Temperature programmed reduction profiles of fresh (1) $Ce_{0.5}Zr_{0.5}O_2$, (2) $Rh/Ce_{0.5}Zr_{0.5}O_2$, (3) $Pt/Ce_{0.5}Zr_{0.5}O_2$, (4) $Pd/Ce_{0.5}Zr_{0.5}O_2$, and recycled (5) $Ce_{0.5}Zr_{0.5}O_2$, (6) $Rh/Ce_{0.5}Zr_{0.5}O_2$, (7) $Pt/Ce_{0.5}Zr_{0.5}O_2$, (8) $Pd/Ce_{0.5}Zr_{0.5}O_2$.

sample (HSA) [2,17]. This effect is even more remarkable in the presence of the supported noble metal, where the reduction of aged samples occurs at a temperature as low as 440 K. Clearly, both textural and structural factors govern the redox behavior of these mixed oxides.

The interpretation of such unusual behavior is given by a comparison of the Raman spectra of fresh and aged $Ce_{0.5}Zr_{0.5}O_2$ (HSA) reported in Fig. 4. Both the fresh metal-free and Rh-loaded $Ce_{0.5}Zr_{0.5}O_2$ (HSA) feature a strong T_{2g} band at 465 cm^{-1} attributed to a totally symmetric M–O (M=Zr, Ce) stretching mode, the intensity of which strongly decreases upon aging in TPR/oxidation processes. This is an indication of a progressive breaking of the symmetry of the M–O bond, leading to an oxygen sublattice as observed in $Ce_{0.5}Zr_{0.5}O_2$ (LSA). Consistently, the Raman spectrum of $Ce_{0.5}Zr_{0.5}O_2$ (LSA) shows four Raman active modes in the ν(M–O) region, suggesting that neither *Fm3m* (cubic fluorite type) nor $P4_2/nmc$ (tetragonal) space group symmetry can be associated with this phase. Such an interpretation is further substantiated by the TPR profiles of the noble metal-loaded HSA $Ce_{0.5}Zr_{0.5}O_2$. In the presence of the noble metal, hydrogen activation is unlikely rate limiting for the reduction process. Consistently, spilling of H_2 to the support surface is responsible for the shift of the surface reduction from 770 to 400–450 K in the HSA CeO_2 in the presence of the noble metal [18]. Accordingly, the reduction peak observed at 880 K for fresh $Ce_{0.5}Zr_{0.5}O_2$ (HSA) shifts to 500–700 K in the presence of Rh, Pt or Pd, leaving the peak at 1100 K unaffected. The sintering occurring in the TPR by modifying the oxygen sublattice increases the oxygen mobility in the bulk, shifting the whole reduction process to low temperatures. As shown by H_2 chemisorption measurements, the higher reduction temperature of aged $Pd/Ce_{0.5}Zr_{0.5}O_2$ (HSA) compared to the Pt- and Rh-containing samples is due to a lower rate of H_2 spillover.

Having established that structural factors and oxygen mobility in the lattice play a key role in determining the redox behavior of CeO_2–ZrO_2 mixed oxides, we recently extended our investigations to ternary systems using trivalent oxides as structural dopants of the mixed oxides [4]. $Ce_{0.6}Zr_{0.4}O_2$ was chosen as the reference mixed oxide since, for this composition, the tetragonal/cubic phase transformation observed for $Ce_{0.5}Zr_{0.5}O_2$ is avoided. The influence of the amount and nature of the trivalent dopant and of aging in consecutive TPR/oxidation cycles was investigated. The critical radius of $Ce_{0.6}Zr_{0.4}O_2$, e.g. the cation radius which produces no cell expansion upon substitution of Zr^{4+}, is about 1 Å. On this basis, we chose the trivalent dopants Ga^{3+}, Y^{3+} and La^{3+}. Of these, the ionic radius of Y^{3+} (1.1015 Å) is very close to the critical radius; Ga^{3+} (0.62 Å) and La^{3+} (1.18 Å) are, respectively, undersized and oversized.

A typical sequence of TPR/oxidation experiments is shown in Fig. 5 for $Ce_{0.6}Zr_{0.375}Y_{0.025}O_{1.9875}$. Noteworthy is the appearance of a single reduction feature observed for the fresh sample, which indicates that reduction occurs concurrently both at the surface and in the bulk of the mixed oxide. In addition, the remarkable modification of

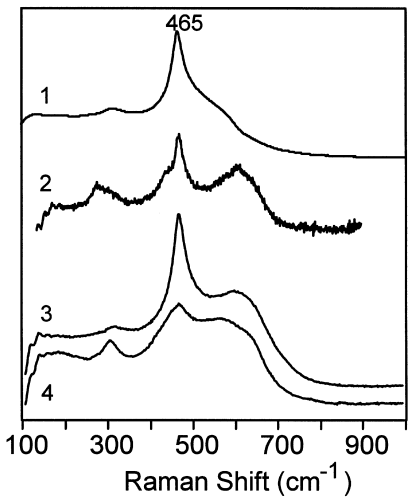

Fig. 4. Raman spectra of (1) fresh and (2) reduced 1000 K/oxidized at 700 K $Ce_{0.5}Zr_{0.5}O_2$, (3) fresh and (4) reduced 1273 K/oxidized at 700 K $Rh/Ce_{0.5}Zr_{0.5}O_2$.

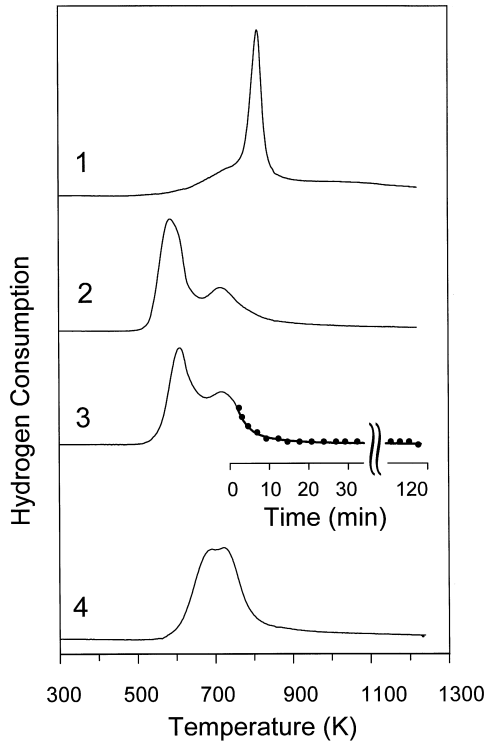

Fig. 5. Temperature programmed reduction of $Ce_{0.6}Zr_{0.375}Y_{0.025}O_{1.9875}$: (1) fresh sample; (2) sample recycled from three consecutive TPRs up to 1273 K and subsequent oxidation at 700 K; (3) TPR up to 750 K followed by isothermal reduction for 2 h of sample recycled from (2); (4) TPR of sample recycled from (3).

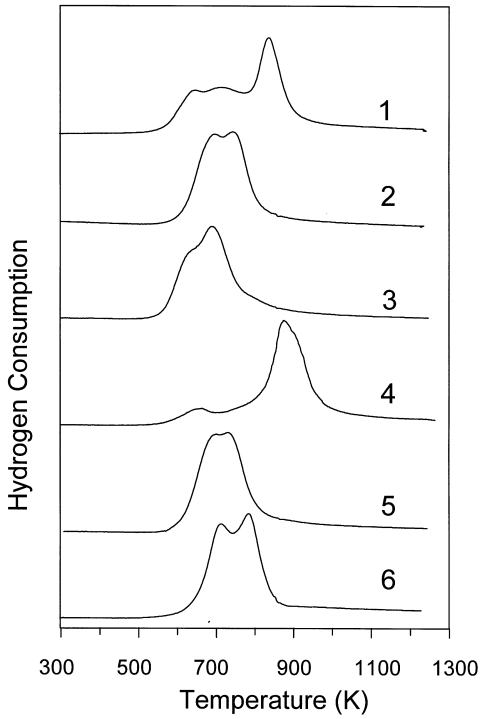

Fig. 6. Temperature programmed reduction of aged samples: (1) $Ce_{0.6}Zr_{0.4}O_2$; (2) $Ce_{0.6}Zr_{0.375}Y_{0.025}O_{1.9875}$; (3) $Ce_{0.6}Zr_{0.35}Y_{0.05}O_{1.975}$; (4) $Ce_{0.6}Zr_{0.30}Y_{0.10}O_{1.95}$; (5) $Ce_{0.6}Zr_{0.375}La_{0.025}O_{1.9875}$; (6) $Ce_{0.6}Zr_{0.375}Ga_{0.025}O_{1.9875}$.

the TPR profiles indicates a significant textural/structural transformation of the mixed oxide which has indeed been detected by N_2 physisorption, Raman and XRD spectra [4]. It is worth noting that we did not detect any further modification of the TPR profile reported in Fig. 5 (trace 4), suggesting that, whatever the modification of the mixed oxide, at this point a stable system is obtained which does not undergo further transformation. The TPR/oxidation cycles lead to a strong sintering of the fresh samples. The reduction profiles of the aged samples are compared in Fig. 6.

The importance of structural design of the redox system in order to obtain high oxygen storage at moderate temperatures appears evident. A perusal of the reduction features reported in Fig. 6 reveals that: (i) an appropriate amount (2.5–5.0 mol%) of trivalent dopant is necessary to achieve a significant improvement in reduction; (ii) among the cations investigated, that with an ionic radius closest to the critical radius of $Ce_{0.6}Zr_{0.4}O_2$ is the most effective in promoting reducibility at low temperature.

Quantitative measurements of oxygen storage carried out on both fresh and aged samples (Table 1) indicate the innovative redox properties of these mixed oxides. All fresh (either LSA or HSA) and aged (HSA) CeO_2–ZrO_2 show very high OSC values due to concurrent reduction both at the surface and in the bulk at moderate temperatures. The independence of OSC of the surface area indicates that these materials are important innovative systems for high temperature TWC applications since sintering does not lead to any significant deactivation of OSC. In contrast, with conventional CeO_2, the OSC at moderate temperatures is conserved only as long as a high surface area is present. As soon as the surface decreases due to the redox cycles, all the low temperature OSC is lost. This makes undoped CeO_2 unsuitable as an oxygen storage device for application in modern TWCs.

This behavior is reflected in both the metal-free and

Table 1
Oxygen uptake (OSC) measured over fresh and aged, doped and undoped NM/CeO_2–ZrO_2 solid solutions (NM = noble metal, dopant = Y^{3+}, Ga^{3+}, La^{3+})

Sample	Reduction temperature	
	1273 K[a] O_2 uptake[c] (% Ce^{3+})	650 K[b] O_2 uptake[c] (% Ce^{3+})
CeO_2 (HSA)	0.50 (35)	0.01 (1)[d]
Rh/CeO_2 (HSA)	0.59 (41)	0.02 (2)[d]
Rh/$Ce_{0.5}Zr_{0.5}O_2$ (LSA)		0.42 (50)
$Ce_{0.5}Zr_{0.5}O_2$ (HSA)	0.53 (63)	0.44 (52)[d]
Rh/$Ce_{0.5}Zr_{0.5}O_2$ (HSA)	0.49 (58)	0.43 (50)[e]
Pt/$Ce_{0.5}Zr_{0.5}O_2$ (HSA)	0.52 (61)	0.45 (54)
Pd/$Ce_{0.5}Zr_{0.5}O_2$ (HSA)	0.53 (63)	0.46 (54)[f]
$Ce_{0.6}Zr_{0.4}O_2$ (HSA)	0.76 (77)	0.46 (46)
$Ce_{0.6}Zr_{0.375}Y_{0.025}O_{1.9875}$ (HSA)	0.76 (77)	0.57 (58)
$Ce_{0.6}Zr_{0.375}La_{0.025}O_{1.9875}$ (HSA)	0.76 (78)	0.58 (59)
$Ce_{0.6}Zr_{0.375}Ga_{0.025}O_{1.9875}$ (HSA)	0.80 (80)	0.57 (58)

[a]TPR of fresh and aged samples carried out up to 1273 K.
[b]Isothermal reduction carried out at the indicated temperature for 2 h on aged samples.
[c]In mmol O_2 g^{-1}, standard deviation ±0.01 mmol O_2 g^{-1}.
[d]Isothermal reduction at 600 K for 2 h.
[e]Isothermal reduction at 440 K for 2 h.
[f]Isothermal reduction at 500 K for 2 h.

noble metal-loaded samples, confirming the importance of the structural doping of CeO_2 with ZrO_2. Finally, a structural modification of $Ce_{0.6}Zr_{0.4}O_2$ by addition of trivalent dopant results in a 30% improvement of the OSC after reduction at 700 K, suggesting that tunable redox systems may be obtained by appropriate structural design.

3.2. NO reduction by CO over $Rh/CeO_2–ZrO_2$ and $Rh/CeO_2–ZrO_2–Y_2O_3$ catalysts

NO reduction by CO is a key step in the catalytic control of automotive exhaust. This reaction is responsible for the removal of NO from the exhaust and also contributes to the elimination of CO. Rhodium is added to commercial TWCs due to its ability to specifically enhance NO conversion [19]. The high activity of rhodium for NO removal is associated with its ability to efficiently dissociate NO [19,20]. Laboratory studies show that ceria favorably alters the kinetics of the NO–CO reaction [21]. Therefore, investigation of the effects induced by metal–ceria interactions on the conversions of exhaust is receiving much attention in the literature. Short lived, but highly productive, enhancement of the conversion have been observed over ceria containing TWCs after reductive pretreatment. Typically, after such treatment, light-off temperatures, i.e. 50% conversion of CO and hydrocarbons (HC), are lowered by 50–100 K [22]. Significantly, NO conversion was also enhanced by this pretreatment. Either the creation of highly active sites at the interface between the metal phase and the reduced CeO_2 or the generation of a new active phase formed by migration of the metal into the ceria lattice have been suggested to be responsible for this phenomenon. Recently, metal covering by ceria particles has also been invoked [23].

The activity of Rh-loaded $CeO_2–ZrO_2$ mixed oxides in the reduction of NO with CO was investigated in a flow reactor. All catalysts were reduced for 2 h at 473 K before the catalytic measurements. A conversion vs. temperature reaction profile obtained for freshly reduced (473 K, 2 h) $Rh/Ce_{0.6}Zr_{0.4}O_2$ is shown in Fig. 7. Noticeably, there is initial NO conversion at RT with no observable concomitant CO oxidation. Conversion of both NO and CO starts at about 350 K and increases progressively with temperature up to approximately 470 K where a sudden decrease of activity in NO reduction is observed. This behavior is less pronounced for CO conversion, where an additional plateau of activity is observed around 550 K due to a change of the stoichiometry of the reaction as the product selectivity changes from N_2O to N_2. The peak of activity at 470 K suggests the presence of an active state of the freshly reduced catalyst which is deactivated by steaming in the presence of NO and CO above 500 K. Consistently, in the run-down part of the thermal cycle no such peak is observed for NO conversion (Fig. 7). Note that the active

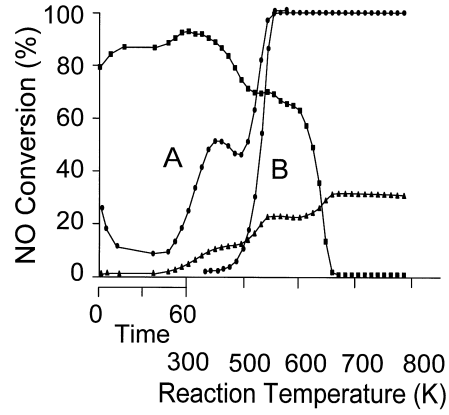

Fig. 7. Reduction of NO with CO over $Rh/Ce_{0.6}Zr_{0.4}O_2$: reaction profile vs. temperature obtained after an initial period of 60 min at 300 K (reaction conditions: NO (1%) and CO (3%) in He, heating/cooling rate 1 K min^{-1}, $W/F=1\times10^{-3}$ $g_{catalyst}$ ml^{-1} min). (■) Selectivity in N_2O formation and (▲) CO conversion measured on a freshly reduced catalyst; (●) NO conversion measured in (A) a run-up experiment on a freshly reduced catalyst, (B) a run-down experiment on an aged catalyst.

state could be regenerated by H_2 treatment at 473 K carried out immediately after the run-down cycle. To investigate the nature and durability of this ''active'' state, the steady state activities were measured for catalysts treated (10–15 h) at 433 or 473 K in the NO/CO stream (1:1, 1 mol% each in He). After this initial period, the catalysts were subjected to consecutive run-up/run-down thermal cycles up to 773 K (heating/cooling rate 1 K min^{-1}), and the steady state activities were again measured. Typically, freshly reduced catalysts show a high initial activity, which slowly (4–6 h) decreases to a stationary value. An initial decrease of catalytic activity is generally observed over supported Rh catalysts [5,24], however compared to Rh/Al_2O_3, strongly enhanced NO conversion is observed initially over reduced $Rh/Ce_{0.5}Zr_{0.5}O_2$: after 5 min on-stream at 473 K (reaction conditions: NO (1%) and CO (1%) in He, $W/F=1\times10^{-3}$ $g_{catalyst}$ ml^{-1} min), NO conversions of 6 and 70% are observed, respectively, for Rh/Al_2O_3 and $Rh/Ce_{0.5}Zr_{0.5}O_2$. The NO conversion initially exceeds that of CO due to an initial NO conversion occurring partly at the expense of Ce^{3+} oxidation. Oxidation of Ce^{3+} to Ce^{4+} was confirmed by in situ XANES spectra recorded at the Ce L_{III} edge; further, no oxygen was detected in the outlet of the reactor.

The steady state activities and apparent activation energies measured during the run-up and run-down cycles are summarized in Table 2. The use of a $CeO_2–ZrO_2$ support clearly improves the activity of the supported rhodium as denoted by the 3–5 times increase of activity compared to Rh/Al_2O_3 (Table 2, runs 1, 3, 5 and 7). This increase of activity is observed for all $CeO_2–ZrO_2$ com-

Table 2
Reaction rates for the NO/CO reaction and apparent activation energies observed over Rh/Al_2O_3, $Rh/CeO_2–ZrO_2$ and $Rh/CeO_2–ZrO_2–Y_2O_3$ catalysts

Run	Support	Pre-treatment	Reaction Rate[a] ($\times 10^9$)	Activation energy[b] (kJ mol^{-1})	
				Run up	Run down
1	Al_2O_3	H_2, 473 K, 2 h	70	115	121
2		NO+CO, 473–773 K	32	134	131
3	$Ce_{0.4}Zr_{0.6}O_2$	H_2, 473 K, 2 h	331	67	93
4		NO+CO, 473–773 K	90	85	87
5	$Ce_{0.6}Zr_{0.4}O_2$	H_2, 473 K, 2 h	336	67	86
6		NO+CO, 473–773 K	46		
7	$Ce_{0.5}Zr_{0.5}O_2$	H_2, 473 K, 2 h	224	66	87
8		NO+CO, 473–773 K	117	118	138
9		NO+CO, 473–773 K[c]	25	129	19
10		H_2, 473 K, 2 h	27	120	146
11		O_2, 700 K, 0.5 h, H_2, 473 K, 2 h	43	123	129
12		O_2, 700 K, 0.5 h, H_2, 1073 K, 2 h	179	86	106
13		NO+CO, 473–773 K	157	92	110
14		NO+CO, 473–773 K[c]	124	94	113
15	$Ce_{0.6}Zr_{0.4}O_2$[d]	H_2, 473 K, 2 h[d]	1630	71	76
16		NO+CO, 433–773 K[d]	1590		
17	$Ce_{0.6}Zr_{0.35}Y_{0.05}O_{1.975}$	H_2, 473 K, 2 h[d]	4500	60	80
18		NO+CO, 473–773 K[d]	2000		

[a]mol NO converted (g catalysts)$^{-1}$ s^{-1}, measured under steady state conditions at 473 K.
[b]Measured during the run-up/run-down cycles in the temperature range 473–530 K; conversion <20%, standard deviation ±8 kJ mol^{-1}.
[c]Aged catalyst.
[d]$Rh(NO_3)_3$ precursor, reaction rate measured at 433 K.

positions employed, indicating that this phenomenon is related to the mixed oxide rather than to the particular composition. An apparent activation energy of 66–67 kJ mol^{-1} is observed for all fresh $CeO_2–ZrO_2$-based catalysts (Table 2, runs 3, 5 and 7), suggesting that a support promoted reaction mechanism is operative under these conditions below 500 K. Prolonged aging in the run-up/run-down cycles, however, gradually deactivates the catalyst to obtain an activity comparable to that of Rh/Al_2O_3 (Table 2, runs 2 and 9). At the same time, the activation energy increases to 129 kJ mol^{-1}, which is comparable to that of Rh/Al_2O_3. Re-activation of the aged catalyst was investigated in detail for $Rh/Ce_{0.5}Zr_{0.5}O_2$ (Table 2, runs 10–12). Both a reduction in H_2 at 473 K and combined mild oxidation/reduction treatment do not re-activate the catalyst significantly, suggesting that the formation of carbon deposits should not be responsible for the partial deactivation. Only when the oxidation is followed by reduction at 1073 K, is re-activation of the catalyst and a ''durable – low temperature active'' state of $Rh/Ce_{0.5}Zr_{0.5}O_2$ again obtained. Such treatment strongly improves the reducibility of the catalyst at low temperatures (compare Section 3.1), suggesting that the redox properties of $Ce_{0.5}Zr_{0.5}O_2$ play a key role in the generation of the ''active'' state. Moreover, reduction at 1073 K leads to a strong sintering of the support, the surface area decreasing from 53 to 18 m^2 g^{-1} [3].

The use of chloride-free precursors dramatically enhances the effectiveness of the ''active'' state of $Rh/CeO_2–ZrO_2$ catalysts (compare Table 2, runs 5 and 15), suggesting that spillover phenomena also play a key role in the $CeO_2–ZrO_2$ mediated reaction mechanism. Chloride is indeed removed with difficulty from CeO_2-based catalysts [25] and it acts as a highly efficient killer of spillover phenomena [26]. Again, the redox properties of the support affect the catalytic efficiency, since by insertion of 5 mol% of Y^{3+} into $CeO_2–ZrO_2$ mixed oxide, the OSC of the system is further improved (compare Section 3.1).

Summarizing, the data show a strong increase of activity over the freshly reduced catalyst which is associated with the ability of $Rh/CeO_2–ZrO_2$ to undergo reduction of the support at low temperatures. The reduction of the catalyst affects the activity mainly in three ways:

1. a strong, transient increase of NO conversion which is already observed at RT;
2. an ''active'' state of the catalyst which exists below 500 K under the reaction conditions and which is reversibly deactivated above this temperature;
3. reduction in H_2 at 1073 K improves the durability and reversibility of the formation of the ''active'' state.

The above findings concerning the ''active'' state of $Rh/CeO_2–ZrO_2$ catalysts can be rationalized in terms of

Ce^{4+}/Ce^{3+} redox couple promoted NO reduction according to the following Scheme:

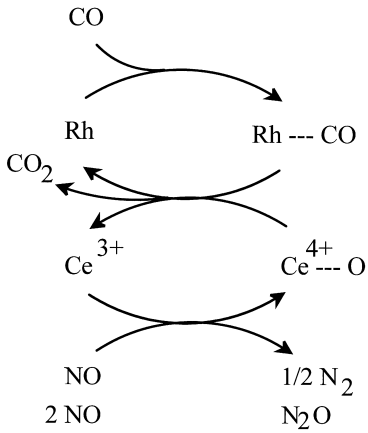

In this scheme, the initial transient high activity is associated with annihilation of the bulk oxygen vacancies created by the initial reduction of the support which provides the driving force for efficient NO reduction to give mainly N_2O [27]. As shown by previous work, reduced ceria containing moieties are easily oxidized by weak oxidants such as CO_2, H_2O and NO [28,29]. Under steady state conditions below 500 K, the Ce^{4+}/Ce^{3+} redox process seems to be related mainly to the surface and near-subsurface regions. Accordingly, the reduction of $Rh/Ce_{0.5}Zr_{0.5}O_2$ at 1073 K does not deactivate the catalyst despite a strong collapse of the surface area. Since Ce^{3+} oxidation at the expense of NO reduction is easy, it seems reasonable that the reduction of Ce^{4+} is the rate limiting step in the scheme. This process is promoted by the supported metal; no catalytic reaction is observed in its absence. The model is further substantiated by the power type dependence of the reaction rates measured for $Rh/Ce_{0.5}Zr_{0.5}O_2$ at 473 K by varying the NO and CO pressure in the range 7–25 Torr. The data can be conveniently fitted to a power type law:

$$\text{Rate (NO conversion)} = k_{NO}\, p(NO)^m p(CO)^n$$

with $k_{NO} = 3.2 \pm 0.5 \times 10^{-8}$ ml $g^{-1}_{catalyst}$ s^{-1}, $m = -2.0 \pm 0.7 \times 10^{-1}$, $n = 2.4 \pm 0.2 \times 10^{-1}$. Pande and Bell reported values of m varying between -3.7×10^{-1} and -1.5×10^{-1} and n varying between 4×10^{-2} and 8×10^{-2} for Rh supported on SiO_2, Al_2O_3 and MgO for the same reaction [30]. The reaction order with respect to p(CO) is significantly higher than observed with the other supports. According to the Scheme, reduction of the CeO_2–ZrO_2 support favors NO conversion. In the presence of H_2, the reduction of the support is promoted via H_2 activation by the supported metal which provides active hydrogen to be spilled over the support favoring reduction. In a CO atmosphere, the formation of carbonates on the CeO_2 surface is observed [31], the desorption of which, leading to reduction of the support, is not an easy process [7]. Rapid CO oxidation occurring at the periphery of the metal particles where the oxygen for CO_2 formation is provided by the nearby support sites is a reasonable model for the reduction process. Under these conditions, the long range effect may become important and oxygen migration towards the metal particles would be rate limiting, as recently proposed by Gorte et al. for CO oxidation over Rh/CeO_2 [32,33]. Consistently, the very high activity of chloride-free catalysts may be attributed to the high efficiency of the reverse spillover of oxygen species. As far as deactivation of the support mediated cycle above 500 K is concerned, it should be noted that this process may be operative as long as the reduced CeO_2–ZrO_2 moiety shows a strong tendency to be oxidized by NO. Nitric oxide adsorption can be used as a valuable tool to determine the presence of reactive oxygen species on the CeO_2 surface [34]. As shown in trace 1 of Fig. 8, NO adsorption at 473 K on pre-reduced $Rh/Ce_{0.5}Zr_{0.5}O_2$ leads to the appearance of a broad IR band centered at 1396 cm^{-1} attributable to nitrite/nitrate species on zirconium sites. In contrast, an equivalent experiment carried out at 523 K does not lead to the formation of nitrite/nitrate species, suggesting the absence of reactive oxygen species in the latter case (Fig. 8, trace 2). Since the catalyst was pre-reduced, the presence of reactive oxygen species is associated with concomitant NO reduction [34]. Their absence after treatment at 523 K suggests that NO reduction leading to reactive surface oxygen species does not proceed at this temperature. Due to the high lability of the surface oxygens at 523 K, surface oxidation by interaction with NO is no longer favored. According to this model the driving force for NO reduction is related to the stability of the surface oxygen vacancies according to the equilibrium:

$$2Ce^{3+} + V_O'' + \tfrac{1}{2}O_2 \rightleftarrows 2Ce^{4+} + O_s$$

where V_O'' and O_s indicate a surface oxygen vacancy and surface oxygen, respectively. Below 500 K, the equilibrium would be shifted to the right which provides the driving force for the reduction of NO. Above 500 K, the equilibrium is shifted to the left and the catalytic cycle mediated by CeO_2–ZrO_2 is deactivated.

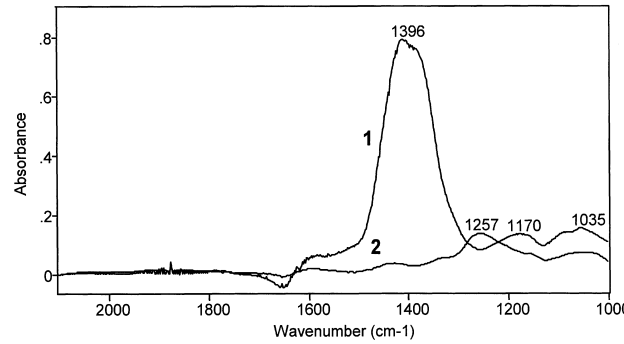

Fig. 8. IR spectra of the adsorption of NO ($p_{NO} = 7$ Torr) on $Rh/Ce_{0.6}Zr_{0.4}O_2$ at (1) 473 K and (2) 523 K.

4. Conclusions

The present work demonstrates the important role of structural doping of CeO_2 with ZrO_2 in modifying both the redox properties (OSC) and catalytic activity in a model TWC reaction. The CeO_2–ZrO_2 systems show high oxygen mobility in the bulk of the solid solution which makes all the redox processes independent of the surface area. This property makes these catalysts thermally stable since no significant deactivation is observed even after extensive sintering. The ability of the Ce^{4+}/Ce^{3+} couple to promote NO reduction at moderate temperatures via an efficient redox type mechanism suggests a possible new interpretation of the role of supported metal in the conversion of NO_x. The high efficiency of sintered catalysts for the reduction of NO by CO also indicates the importance of the near-surface/subsurface region in redox processes, which suggests that highly efficient TWCs may be obtained by a proper structural design of the redox system.

Acknowledgements

The Mìnistero dell'Ambiente (Roma) and Università di Trieste are acknowledged for financial support.

References

[1] B.J. Cooper, W.D.J. Evans, B. Harrison, Catalysis and Automotive Pollution Control I, Elsevier, Amsterdam, 1987, p. 117.
[2] P. Fornasiero, G. Balducci, R. Di Monte, J. Kašpar, V. Sergo, G. Gubitosa, A. Ferrero, M. Graziani, J. Catal. 164 (1996) 173.
[3] P. Fornasiero, J. Kašpar, M. Graziani, J. Catal. 167 (1997) 576.
[4] P. Vidmar, P. Fornasiero, J. Kašpar, M. Graziani, J. Catal. 171 (1997) 160.
[5] J. Kašpar, C. de Leitenburg, P. Fornasiero, A. Trovarelli, M. Graziani, J. Catal. 146 (1994) 136.
[6] V. Perrichon, A. Laachir, G. Bergeret, R. Frety, L. Tournayan, O. Touret, J. Chem. Soc., Faraday Trans. 90 (1994) 773.
[7] A. Laachir, V. Perrichon, A. Badri, J. Lamotte, E. Catherine, J.C. Lavalley, J. El Fallah, L. Hilaire, F. Le Normand, E. Quemere, N.S. Sauvion, O. Touret, J. Chem. Soc., Faraday Trans. 87 (1991) 1601.
[8] J. El Fallah, S. Boujana, H. Dexpert, A. Kiennemann, J. Majerus, O. Touret, F. Villain, F. Le Normand, J. Phys. Chem. 98 (1994) 5522.
[9] H.C. Yao, Y.F. Yu Yao, J. Catal. 86 (1984) 254.
[10] J.L.G. Fierro, J. Soria, J. Sanz, J.M. Rojo, J. Solid State Chem. 66 (1987) 154.
[11] M. Ozawa, M. Kimura, A. Isogai, J. Alloys Comp. 193 (1993) 73.
[12] T. Murota, T. Hasegawa, S. Aozasa, H. Matsui, M. Motoyama, J. Alloys Comp. 193 (1993) 298.
[13] G. Ranga Rao, J. Kašpar, R. Di Monte, S. Meriani, M. Graziani, Catal. Lett. 24 (1994) 107.
[14] P. Fornasiero, R. Di Monte, G. Ranga Rao, J. Kašpar, S. Meriani, A. Trovarelli, M. Graziani, J. Catal. 151 (1995) 168.
[15] G. Vlaic, P. Fornasiero, S. Geremia, J. Kašpar, M. Graziani, J. Catal. 168 (1997) 386.
[16] C. de Leitenburg, A. Trovarelli, F. Zamar, S. Maschio, G. Dolcetti, J. Llorca, J. Chem. Soc., Chem. Commun. (1995) 2181.
[17] G. Balducci, P. Fornasiero, R. Di Monte, J. Kašpar, S. Meriani, M. Graziani, Catal. Lett. 33 (1995) 193.
[18] B. Harrison, A.F. Diwell, C. Hallett, Plat. Met. Rev. 32 (1988) 73.
[19] K.C. Taylor, Catal. Rev. Sci. Eng. 35 (1993) 457.
[20] M. Shelef, G.W. Graham, Catal. Rev. Sci. Eng. 36 (1994) 433.
[21] S.H. Oh, J. Catal. 124 (1990) 477.
[22] J.G. Nunan, H.J. Robota, M.J. Cohn, S.A. Bradley, J. Catal. 133 (1992) 309.
[23] S.E. Golunski, H.A. Hatcher, R.R. Rajaram, T.J. Truex, Appl. Catal. B, Environ. 5 (1995) 367.
[24] W.C. Hecker, A.T. Bell, J. Catal. 84 (1983) 200.
[25] S. Bernal, F.J. Botana, J.J. Calvino, M.A. Cauqui, G.A. Cifredo, A. Jobacho, J.M. Pintado, J.M. Rodriguez-Izquierdo, J. Phys. Chem. 97 (1993) 4118.
[26] R. Taha, D. Martin, S. Kacimi, D. Duprez, Catal. Today 29 (1996) 89.
[27] G. Ranga Rao, P. Fornasiero, R. Di Monte, J. Kašpar, G. Vlaic, G. Balducci, S. Meriani, G. Gubitosa, A. Cremona, M. Graziani, J. Catal. 162 (1996) 1.
[28] C. Padeste, N.W. Cant, D.L. Trimm, Catal. Lett. 28 (1994) 301.
[29] A. Trovarelli, G. Dolcetti, C. de Leitenburg, J. Kašpar, P. Finetti, A. Santoni, J. Chem. Soc., Faraday Trans. 88 (1992) 1311.
[30] N.K. Pande, A.T. Bell, J. Catal. 98 (1986) 7.
[31] A. Badri, J. Lamotte, J.C. Lavalley, A. Laachir, V. Perrichon, O. Touret, N.S. Sauvion, E. Quemere, Eur. J. Solid State Inorg. Chem. 28 (1991) 445.
[32] T. Bunluesin, H. Cordatos, R.J. Gorte, J. Catal. 157 (1995) 222.
[33] H. Cordatos, T. Bunluesin, J. Stubenrauch, J.M. Vohs, R.J. Gorte, J. Phys. Chem. 100 (1996) 785.
[34] A. Martinez-Arias, J. Soria, J.C. Conesa, X.L. Seoane, A. Arcoya, R. Cataluna, J. Chem. Soc., Faraday Trans. 91 (1995) 1679.
[35] M. Yashima, H. Arashi, M. Kakihana, M. Yoshimura, J. Am. Ceram. Soc. 77 (1994) 1067.
[36] M. Yashima, K. Morimoto, N. Ishizawa, M. Yoshimura, J. Am. Ceram. Soc. 76 (1993) 1745.